Available online at www.sciencedirect.com
SCIENCE DIRECT®
Polyhedron 24 (2005) 41–48
POLYHEDRON
www.elsevier.com/locate/poly

Bis(μ-alkoxo)-bridged dinuclear iron(III) complexes of pyrazole-based ligands as models for iron-oxo proteins

Stefania Tanase [a], Elisabeth Bouwman [a], Gary J. Long [b], Ahmed M. Shahin [b], René de Gelder [c], Allison M. Mills [d], Anthony L. Spek [d], Jan Reedijk [a,*]

[a] Leiden Institute of Chemistry, Gorlaeus Laboratories, Leiden University, P.O. Box 9502, 2300 RA Leiden, The Netherlands
[b] Department of Chemistry, University of Missouri-Rolla, Rolla, MO 65409-0010, USA
[c] Institute for Molecules and Materials, Radboud University, Nijmegen, Toernooiveld 1, 6525 ED Nijmegen, The Netherlands
[d] Bijvoet Center for Biomolecular Research, Utrecht University, Padualaan 8, 3584 CH Utrecht, The Netherlands

Received 19 May 2004; accepted 27 July 2004
Available online 21 November 2004

Abstract

The synthesis and characterization of two new bis(μ-alkoxo)-bridged dinuclear iron(III) complexes with the ligands 1-(2-hydroxyethyl)-pyrazole (Hnhep) and 1-(2-hydroxyethyl)-3,5-dimethylpyrazole (Hnhed), $[Fe(nhep)Cl_2(EtOH)]_2$ (**1**) and $[Fe(nhed)Cl_2]_2$ (**2**) are reported. The crystal structures of both complexes reveal the presence of centrosymmetric dinuclear units. In compound **1**, the iron(III) center has a coordination number of six, with a slightly distorted octahedral geometry. In compound **2**, the bulkier nhed ligand, with methyl groups at the 3- and 5-positions of the pyrazole ring, leads to a coordination number of five at the iron(III) center in a distorted square pyramidal geometry. The magnetic properties of both complexes have been investigated in the range 2–300 K and indicate the presence of fairly weak antiferromagnetic exchange interactions between iron(III) ions ($J_1 = -10.04$ cm^{-1} for **1** and $J_2 = -12.5$ cm^{-1} for **2**). The inactivity of both complexes in the cyclohexane hydroxylation appears to be partly due to the presence of the strong iron(III)–chloride bond that does not allow exchange with the reactant molecules.

Keywords: Iron; Pyrazole; Alkoxo-bridged; Model compounds

1. Introduction

Over the past few decades, considerable progress has been made in the development of oxo-bridged dinuclear iron(III) complexes that can reproduce both the structural and the functional properties of the metallic cores of the non-heme proteins including hemerytin (Hr) [1], ribonucleotide reductase (RR) [2], methane monooxygenase (MMO) and purple acid phosphatase (PAPs) [3]. In particular, the ability of the MMO enzyme to activate inert C–H bonds under ambient conditions has received special attention over the past 20 years. The enzyme is known to catalyze the conversion of methane into methanol (Eq. (1)). Substrate oxidation occurs at the diiron centre of the hydroxylase component of the enzyme, which receives two electrons from NADH via reductase to activate the dioxygen molecule [4].

$$2NADH + CH_4 + O_2 \rightarrow 2NAD^+ + CH_3OH + H_2O + 2e^- \quad (1)$$

In the oxidized state of methane monooxygenase (MMO_{ox}), the positive charge of the two high-spin iron(III) ions is balanced by four glutamate and two bridging hydroxide ligands; two additional histidine ligands complete the octahedral coordination spheres of the iron ions [5]. Because of the rather elaborate synthesis

* Corresponding author. Tel.: +31 715274450; fax: +31 715274671.
E-mail address: reedijk@chem.leidenuniv.nl (J. Reedijk).

0277-5387/$ - see front matter © 2004 Published by Elsevier Ltd.
doi:10.1016/j.poly.2004.07.026

of imidazole-based ligands, aliphatic amines, imine or pyridines are commonly used to synthesize model compounds [3,6–11]. Pyrazole-based ligands have been less well investigated for the purpose of synthesizing model complexes that can mimic the active site of those metalloenzymes and metalloproteins which are known to contain imidazole groups from histidine bound to the iron center in the active site [12,13]. This type of ligands might be preferred in the field of biomimetic chemistry, both because they are good structural analogues for the size and electronic properties of histidine and because of their relative ease of preparation as compared to imidazole ligands.

Although a large number of oxygen-bridged dinuclear iron(III) complexes have been synthesized and characterized as structural and functional models for the MMO enzyme, the most efficient models for alkane hydroxylation remain μ-oxo dinuclear iron(III) complexes with didentate (bipyridine, bpy) [10,14], or tetradentate (tris(2-pyridylmethyl)amine, tpa) pyridine-like ligands [7,15–17] and exchangeable μ-acetato or terminal aquo ligands. In these cases, both *tert*-butylhydroperoxide and H_2O_2 have proven to be the most widely studied oxidants in association with these catalysts. In a programme to search for more adequate synthetic models for the active site of MMO, we report herein the synthesis, characterization, magnetic properties and the reactivity studies of two new bis(μ-alkoxo)-bridged dinuclear iron(III) complexes, $[Fe(nhep)Cl_2(EtOH)]_2$ (**1**) (Hnhep = 1-(2-hydroxyethyl)-pyrazole) and $[Fe(nhed)Cl_2]_2$ (**2**) (Hnhed = 1-(2-hydroxyethyl)-3,5-dimethylpyrazole).

2. Experimental

2.1. Synthesis

Chemicals were purchased from Aldrich and were used as received. The ligands 1-(2-hydroxyethyl)-pyrazole (Hnhep) [18] and 1-(2-hydroxyethyl)-3,5-dimethylpyrazole (Hnhed) [19] were synthesized as previously reported.

2.1.1. $Fe(nhep)Cl_2(EtOH)]$ (**1**)

The complex was obtained by slow diffusion, in an H-shaped tube, of two ethanolic solutions, one containing 1 mmol (0.2 g) $FeCl_2 \cdot 4H_2O$ and the other one containing 1 mmol (0.15 g) of 1-(2-hydroxyethyl)-pyrazole. Dark orange crystals were obtained in one week. The crystals were collected by filtration, washed with diethyl ether and dried in vacuum. Yield: 0.32 g (60%) *Anal.* Calc. for $C_{14}H_{26}Cl_4Fe_2N_4O_4$: C, 29.57; H, 4.57; N, 9.85. Found: C, 29.89; H, 4.62; N, 9.48%. IR (ν_{max}/cm^{-1}): 3288m, 2938m, 2873w, 1624w, 1546m, 1421s, 1280m, 1188s, 1060s, 1028s, 1004m, 893s, 765s, 611m, 562s, 467s, 386m. UV–Vis (λ_{max}/nm): 411, 639, 1050.

2.1.2. $Fe(nhed)Cl_2]$ (**2**)

The complex was prepared by adding 2 mmol (0.3 g) of the ligand 1-(2-hydroxyethyl)-3,5-dimethylpyrazole (Hnhed) dissolved in 10 ml of tetrahydrofuran to a solution of 2 mmol (0.4 g) $FeCl_2 \cdot 4H_2O$ in 20 ml tetrahydrofuran. Slow diffusion of hexane into the resulting orange solution over 3 days yielded orange crystals that were collected by filtration, washed with hexane and dried in air. Yield: 0.45 g (78%) *Anal.* Calc. for $C_{14}H_{22}Cl_4Fe_2N_4O_2$: C, 30.45; H, 3.98; N, 10.15. Found: C, 31.07; H, 3.74; N, 10.48%. IR (ν_{max}/cm^{-1}): 2925m, 2865w, 1636w, 1558m, 1473s, 1364m, 1227m, 1133s, 1084m, 1049s, 895s, 798s, 627m, 570s, 513m, 450s, 356m. UV–Vis (λ_{max}/nm): 407, 589, 1018.

2.2. Physical measurements

Elemental analyses of C, H, and N were performed on a Perkin Elmer 2400 Series II analyzer. Infrared spectra (4000–300 cm^{-1}) were recorded using the reflectance technique on a Perkin–Elmer Paragon 1000 FTIR spectrometer equipped with a Golden Gate ATR device. Ligand field spectra were obtained on a Perkin-Elmer Lambda 900 spectrophotometer using the diffuse reflectance technique, with MgO as a reference. Magnetic susceptibility measurements (2–300 K) were carried out at 1 T using a Quantum Design MPMS-5 5T SQUID magnetometer. Data were corrected for the magnetization of the sample holder and for diamagnetic contributions, the latter of which were calculated from the Pascal constants [20]. The GC–MS measurements were carried out on a Hewlett–Packard 5890 Series II gas chromatograph, equipped with WCOT fused silica column (stationary phase: CP-Was 58 (FFAP) CB) and coupled to a Hewlett–Packard 5971 series mass spectrometer with a mass-selective detector. Standard oxidation reactions were carried out under ambient conditions. The Mössbauer spectra were measured on a constant-acceleration spectrometer which utilized a room temperature rhodium matrix cobalt-57 source and was calibrated at room temperature with α-iron foil.

2.3. X-ray crystallography and data collection

Intensity data for a single crystals of **1** and **2** were collected using Mo Kα radiation (λ = 0.71073 Å) on a Nonius KappaCCD diffractometer. A correction for absorption was considered unnecessary in the case of compound **1**. In the case of compound **2**, an empirical absorption correction was made using PLATON/DELABS (0.600–0.800 transmission) [21]. The structures were solved by automated Patterson methods using DIRDIF99 (**1**) or direct methods using SHELX-97 (**2**) and were refined on F^2 by least-squares procedures using SHELXL-97 [22–24]. All non-hydrogen atoms were refined with anisotropic displacement parameters. In the

case of compound **1**, all hydrogen atoms were independently refined. For compound **2**, all hydrogen atoms were constrained to idealized geometries and allowed to ride on their carrier atoms with an isotropic displacement parameter related to the equivalent displacement parameter of their carrier atoms. Structure validation and molecular graphics preparation were performed with the PLATON package [21].

2.4. Oxidation reactions

2.4.1. Procedure I

In a typical run, 10 equiv. of H_2O_2 (30%) were added to a methanol solution (10 ml) containing 1 mM catalyst (stock solution) and 1 M cyclohexane at room temperature with a final catalyst:substrate:H_2O_2 ratio of 1:1000:10.

2.4.2. Procedure II

The complexes (0.05 mmol) were dissolved in methanol (10 ml) containing 2.5 mmol of substrate. The reaction was started by adding 5 mmol of 30% H_2O_2. The final catalyst:substrate:H_2O_2 ratio was 1:50:100. In both procedures, after 3 h of reaction at 25 °C, aliquots were taken from the reaction mixtures and analyzed twice by GC–MS: both with and without the addition of an excess of triphenylphosphane for the quantification of the amount of hydroperoxide [25]. Chlorobenzene was used as internal standard.

3. Results and discussions

3.1. Synthesis and spectroscopic studies

The reaction of Hnhep or Hnhed with either $FeCl_2$ or $FeCl_3$ affords two new bis(μ-alkoxo)-bridged dinuclear iron(III) complexes (**1** and **2**), as confirmed by their X-ray structure determinations (vide infra).

The infrared spectra of the complexes **1** and **2** exhibit the bands expected for the deprotonated ligands 1-(2-oxyethyl)-pyrazole and 1-(2-oxyethyl)-3,5-dimethylpyrazole. The most significant effect of the coordination of the pyrazole-based ligands to the iron(III) center is observed in the range 1500–1650 cm^{-1}. In this spectral range, both free ligands exhibit two characteristic bands, ν(C=N) (at 1636 cm^{-1} for Hnhep and 1642 cm^{-1} for Hnhed) and ν(C–O) (at 1508 cm^{-1} for Hnhep and 1512 cm^{-1} for Hnhed). Upon coordination of these ligands to iron(III), the energy of the ν(C=N) band decreases (to 1624 cm^{-1} for **1** and 1632 cm^{-1} for **2**) and that of ν(C–O) increases (to 1546 cm^{-1} for **1** and 1558 cm^{-1} for **2**), suggesting the presence of an alkoxo bridge. Both the symmetric and the asymmetric Fe–O–Fe vibrations have associated bands in the infrared spectra of complexes **1** and **2** [26]. The asymmetric stretching vibrations at 611 cm^{-1} for **1** and 627 cm^{-1} for **2** and the symmetric stretching vibrations at 562 cm^{-1} for **1** and 570 cm^{-1} for **2** are in the range of those observed for similar $Fe_2(OR)_2$ dimers [3,6–11]. A sharp peak at 3288 cm^{-1} observed in the infrared spectrum of **1** indicates the presence of moderately strong hydrogen bonds.

The ligand field spectra of both **1** and **2** display the features typical of bis(μ-alkoxo)-bridged iron(III) compounds: an intense absorption band (at 411 nm for **1** and 407 nm for **2**) with a lower energy shoulder (at 639 nm for **1** and 589 nm for **2**), assigned to the ligand-to-iron(III) charge-transfer transitions [27]. In the ligand field spectrum of complex **2**, a medium intensity absorption band that occurs at 1018 nm is attributed to the d–d transitions involving forbidden states of high-spin iron(III). The unusually high intensity of this band may be due either to the exchange coupling between the iron(III) centers that engenders a relaxation of the spin selection rules or to the low symmetry of the iron(III) coordination [28]. For complex **1**, a weak poorly-resolved absorption band at 1050 nm is observed.

3.2. Description of crystal structures

The structures of complexes **1** and **2** were determined by X-ray crystallography. Crystallographic data and selected bond lengths and angles are listed in Tables 1 and 2.

A Pluton projection of the centrosymmetric dinuclear unit of **1** is depicted in Fig. 1. Each iron center, coordinated to two bridging alkoxo-groups, two terminal chloride ions, one nitrogen atom of the Hnhep pyrazole ring and one oxygen atom of an ethanol molecule, has a Cl_2NO_3 donor set in a pseudo-octahedral geometry. The two metal-centred octahedra share an edge in the dinuclear complex. The anionic Hnhep ligand is found in a didentate coordination mode forming the alkoxo-bridges of a planar $Fe_2(OR)_2$ core. The O6–Fe1–N1 bite angle (87.78(5)°) is smaller than that found in a related copper compound [29]. The Fe1–O_{alkoxo} bond distances of 1.9707(10) and 2.0026(10) Å are nearly equivalent to those observed in other bis(μ-alkoxo)-iron complexes [30–33]. The Fe–O–Fe angle (105.69(5)°) and the Fe···Fe separation (3.1670(5) Å) are within the range of values found in bis(μ-alkoxo)-bridged iron(III) complexes [26,30,31,33]. The positions of *trans* coordinating ligands deviate slightly from linearity (161.75(5)°–175.67(4)°), and the iron(III) ion is lifted from the basal plane by 0.17 Å in the direction of the ethanol molecule. The two chloride ions are *cis* to each other (Cl1–Fe1–Cl2 = 93.936(19)°) with Fe–Cl bond distances of 2.2667(5) and 2.3400(5) Å that are close to the values generally observed for iron(III) complexes [34–38]. An interesting feature of the crystal structure of **1** is the presence of two intramolecular hydrogen bonds (Fig. 1) that are established between the chloride ions

Table 1
Crystal and structure refinement data

	$[Fe(nhep)Cl_2(EtOH)]_2$ (**1**)	$[Fe(nhed)Cl_2]_2$ (**2**)
Chemical formula	$C_{14}H_{26}Cl_4Fe_2N_4O_4$	$C_{14}H_{22}Cl_4Fe_2N_4O_2$
Molecular weight	567.89	531.86
Crystal system	monoclinic	monoclinic
Space group	$P2_1/c$	$P2_1/c$
a (Å)	8.9777(11)	11.1114(3)
b (Å)	11.7553(11)	9.4134(2)
c (Å)	12.7193(14)	10.8790(2)
β (°)	125.156(7)	112.1261(9)
V (Å^3)	1097.5(2)	1054.10(4)
Z	2	2
D_{calc} (Mg m^{-3})	1.7185(3)	1.6757(1)
μ(Mo Kα) (mm^{-1})	1.836	1.899
Crystal size (mm)	$0.23 \times 0.21 \times 0.19$	$0.24 \times 0.24 \times 0.12$
T (K)	293(2)	150
Data collected	38 599	11 672
Unique data	2527	2391
R_{int}	0.0371	0.0412
$R(F)$ [$I > 2\sigma(I)$]	0.0216	0.0270
$R_w(F^2)$	0.0496	0.0621
S	1.03	1.03
$\Delta\rho_{min}$, $\Delta\rho_{max}$ (e Å^{-3})	0.284, −0.245	0.285, −0.313

Table 2
Selected bond distances (Å) and angles (°)

$[Fe(nhep)Cl_2(EtOH)]_2$ (**1**)		$[Fe(nhed)Cl_2]_2$ (**2**)	
Bond distances			
Fe1–Cl1	2.3400(5)	Fe1–Cl1	2.2490(6)
Fe1–Cl2	2.2667(5)	Fe1–Cl2	2.2183(6)
Fe1–O6	2.0026(10)	Fe1–O10	1.9384(13)
Fe1–O9	2.1796(13)	Fe1–N12	2.1059(16)
Fe1–N1	2.1106(13)	Fe1–O10a	2.0157(13)
Fe1–O6a	1.9707(10)	Fe···Fe	3.184
Fe···Fe	3.167		
Bond angles			
Cl1–Fe1–Cl2	93.936(19)	Cl1–Fe1–Cl2	112.05(2)
Cl1–Fe1–O6	95.46(4)	Cl1–Fe1–O10	132.86(5)
Cl1–Fe1–O9	175.67(4)	Cl1–Fe1–N12	94.86(5)
Cl1–Fe1–N1	91.71(4)	Cl1–Fe1–O10a	91.75(4)
Cl1–Fe1–O6a	93.44(4)	Cl2–Fe1–O10	113.38(5)
Cl2–Fe1–O6	169.78(4)	Cl2–Fe1–N12	102.45(5)
Cl2–Fe1–O9	89.43(4)	Cl2–Fe1–O10a	94.74(5)
Cl2–Fe1–N1	95.96(4)	O10–Fe1–N12	87.23(6)
Cl2–Fe1–O6a	101.14(3)	O10–Fe1–O10a	72.75(6)
O6–Fe1–O9	81.39(5)	N12–Fe1–O10a	157.64(6)
O6–Fe1–N1	87.78(5)		
O6–Fe1–O6a	74.31(5)		
O9–Fe1–N1	85.22(5)		
O9–Fe1–O6a	88.58(5)		
N1–Fe1–O6a	161.75(5)		

Symmetry operations: x, y, z; $-x$, 1/2 + y, 1/2−z; $-x$, $-y$, $-z$; x, −1/2 + y, −1/2 + z.

and the ethanol molecules of the adjacent iron(III) centers (O9–H9···Cl1a = 3.163(2) Å). The observed O-H stretching vibration of the ethanol molecule (3288 cm^{-1}) and the O–H···Cl distance fit fairly well the relationship developed by Bellamy et al. (O9–H9···Cl1a = 3.158 Å) [39]. No evidence was found for strong intermolecular contacts between dinuclear units.

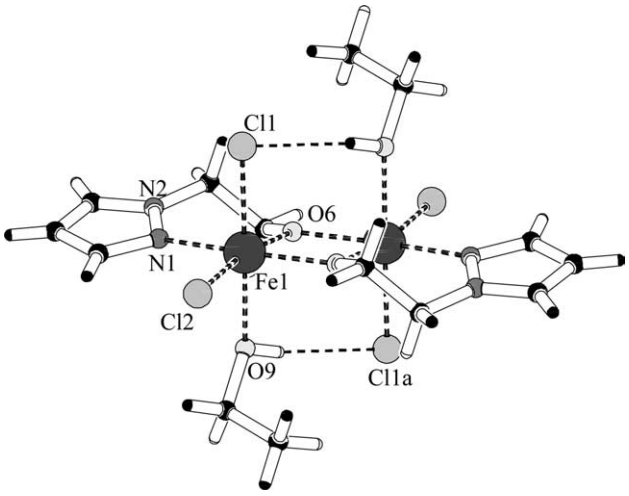

Fig. 1. Pluton projection and numbering scheme of the dinuclear structure of **1**.

The crystal structure of compound **2** (Fig. 2) reveals a centrosymmetric dinuclear unit, similar to that observed for compound **1**. The presence of the methyl groups at the 3- and 5-positions of the pyrazole ring of the Hnhed ligand in **2** results in a change of the coordination geometry around the iron(III) ions. Each iron(III) center is now five-coordinate and has a distorted square pyramidal geometry (as ascertained by the factor $\tau = 0.4$; $\tau = 0$ for a square pyramid and $\tau = 1$ for trigonal bipyramid) [40]. One chloride ion, the two bridging O_{alkoxo} ligands and the nitrogen donor of the pyrazole ring constitute the basal plane of the square pyramid, and the other chloride ion occupies the apical position of the square pyramid. As a result, the dinuclear complex consists of two square pyramids sharing a basal edge (Fig. 2). The largest distortion from the square pyramidal geometry is evidenced by the angles N12–Fe1–O10a = 157.64(6)° and O10–Fe1–Cl1 = 72.75(6)°. The O10–Fe1–N12 = 87.23(6)° bite angle of the didentate ligand is similar to that observed for Hnhep in compound **1**.

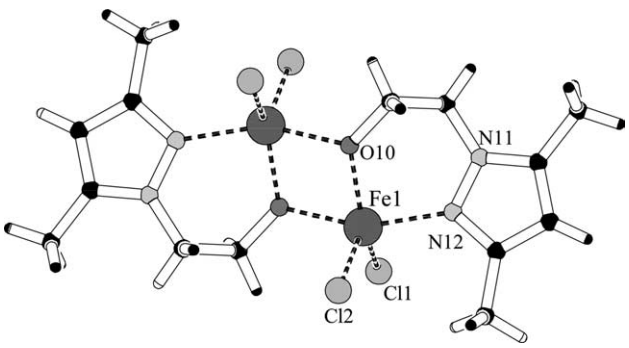

Fig. 2. Pluton projection and numbering scheme of the dinuclear structure of **2**.

The Fe–O–Fe angle (107.25(6)°), Fe–O distances (1.9384(14) and 2.0157(16) Å) and Fe···Fe separation (3.184 Å) are within the range of values found for related bis(μ-alkoxo) bridged iron(III) complexes [30–32,41]. The angle between the two chloride ions is Cl1–Fe1–Cl2 = 112.05(2)°; the average Fe–Cl bond distance of 2.2336(5) Å, is significantly shorter than in compound **1**, but still within the range of the values observed for other iron(III) complexes [34–38]. No stacking interactions or classical hydrogen bonds are observed in the crystal structure of compound **2**.

3.3. Magnetic properties

The variable temperature solid-state magnetic susceptibilities of **1** and **2** have been investigated in the range 2–300 K in an applied magnetic field of 1 T. The values of the $\chi_m T$ product at room temperature are 8.761 $cm^3\,K\,mol^{-1}$ for **1** and 8.749 $cm^3\,K\,mol^{-1}$ for **2**, in agreement with the expected value for two independent spins $S = 5/2$ (8.754 $cm^3\,K\,mol^{-1}$). The $\chi_m T$ versus T curves of both compounds are similar and show a continuous decrease, as the temperature is lowered from 300 to 2 K indicating that the two iron(III) ions are antiferromagnetically coupled. Fig. 3 shows the $\chi_m T$ versus T plot for compound **1**; a very similar behaviour was observed for **2** (not shown).

The six possible states for a dinuclear Fe(III)–Fe(III) complex have total spins of $S = 0, 1, 2, 3, 4, 5$. These spin states are split in energy and produce a spin ladder that can be modeled by the Heisenberg–Dirac–van Vleck phenomenological Hamiltonian: $H = -2JS_1S_2$ [20]. The value of the exchange interaction J can be obtained from the fit of the $\chi_m T$ versus T curve, where the measured magnetic susceptibility is a sum of three terms without zero field splitting (Eq. (2)):

$$\chi_{exp} = \chi_{para} + \chi_{dia} + \chi_{TIP} \tag{2}$$

in which χ_{para} is the paramagnetic (temperature-dependent) contribution, χ_{dia} is the diamagnetic contribution and χ_{TIP} is the temperature-independent paramagnetism, arising from mixing of the excited states into the ground state by the magnetic field. Typically J is determined from a fit of the magnetic susceptibility data using the Van Vleck equation evaluated for an exchange-coupled high-spin dinuclear Fe(III)Fe(III) complex (Eq. (3)) [20]:

$$\chi = \frac{2Ng^2\beta^2}{kT} \times \frac{e^x + 5e^{3x} + 14e^{6x} + 30e^{10x} + 55e^{15x}}{1 + 3e^x + 5e^{3x} + 7e^{6x} + 9e^{10x} + 11e^{15x}}, \tag{3}$$

with $x = J/kT$. The temperature-independent paramagnetism (TIP = 400×10^{-6} $cm^3\,K\,mol^{-1}$ for each iron ion) was taken into account. Using this approach, the best fit parameters were $J_1 = -10.04$ cm^{-1}, $g_1 = 2.02$, for compound **1** and $J_2 = -12.5$ cm^{-1}, $g_2 = 2.03$, for compound **2**. The values obtained are in the range of those observed for other weak antiferromagnetically coupled alkoxo-iron complexes. A correlation between the experimental and calculated magnetic data together with structural parameters is shown in Table 3 [42].

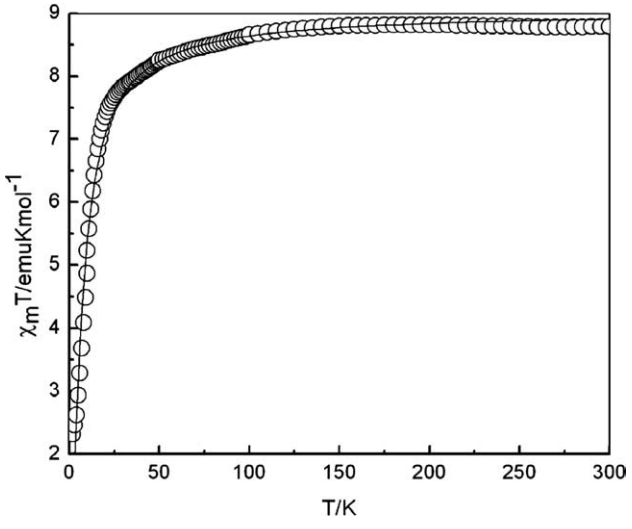

Fig. 3. Plot of the χ_mT vs. T for compound **1**: circles experimental values; (—) calculated values.

3.4. Mössbauer spectral studies

The Mössbauer spectra of **1** and **2** have been measured at 295 and 78 K and show the expected single quadrupole doublet. The hyperfine parameters resulting from quadrupole doublet fits are given in Table 4 and the 78 K spectra are shown in Fig. 4. The 295 K spectra are essentially identical to the 78 K spectra. The hyperfine parameters are typical of iron(III) [43–45] in a somewhat distorted five- or six-coordinate environment and, as expected, the isomer shifts increase slightly upon cooling as a result of the second-order Doppler shift. Rather surprisingly there is little difference in the isomer shift between the six-coordinate iron(III) in **1** and the

Table 3
Magnetic and structural parameters

Complex	P (Å)[a]	d(Fe···Fe) (Å)	α (°)[b]	J_{calc} (cm^{-1})[c]	J_{exp} (cm^{-1})
1	1.9708	3.167	105.69	−12.7	−10
2	1.9384	3.184	107.25	−19.5	−12.5

[a] P corresponds to the half of the length of the shortest Fe–O–Fe bridge.
[b] α = Fe–O–Fe angle.
[c] Calculated after Gorun and Lippard [42] ($-J = Ae^{BP}$) with $A = -1.08 \times 10^{13}$ cm^{-1} and $B = -13.9$ $Å^{-1}$.

Table 4
Mössbauer spectral hyperfine parameters

Compound	T (K)	δ (mm/s[a])	ΔE_Q (mm/s)	Γ (mm/s)	Area ((%ε)/(mm/s))
$[Fe(nhep)Cl_2(EtOH)]_2$ (**1**)	295	0.314(6)	0.40(2)	0.31(1)	0.45(2)
	78	0.409(3)	0.47(1)	0.25(1)	1.64(1)
$[Fe(nhed)Cl_2]_2$ (**2**)	295	0.320(6)	0.51(2)	0.31(1)	1.54(2)
	78	0.412(4)	0.54(1)	0.31(1)	2.33(1)

[a] The isomer shifts are given relative to room temperature α-iron foil.

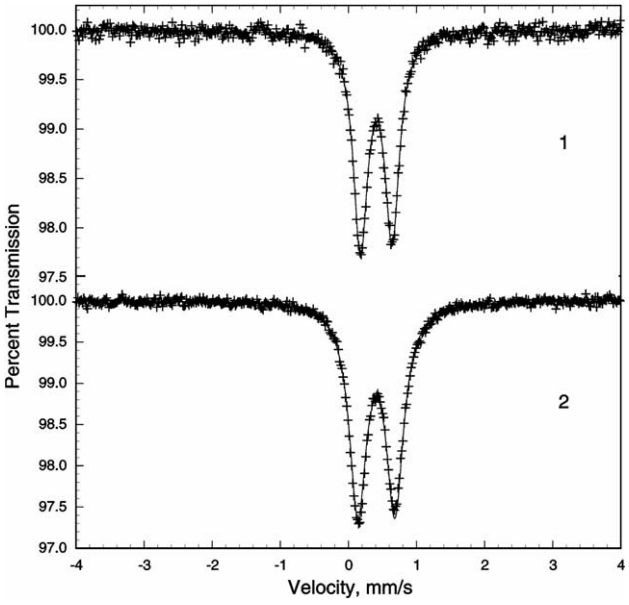

Fig. 4. The Mössbauer spectra of **1** and **2** obtained at 78 K.

five-coordinate iron(III) in **2**, but the five-coordinate **2** does exhibit a slightly larger quadrupole splitting.

3.5. Reactivity studies

The monooxygenase-like activity of complexes **1** and **2** has been tested in the oxidation of cyclohexane using H_2O_2 as oxidant, in methanol as solvent, and under ambient conditions. However, by using either one of the procedures described in the experimental part, no cyclohexane conversion was observed. Several additives (*N*-methylimidazole, acetic acid, benzoic acid, pyridine 2-carboxylic acid, pyridine 2,6-dicarboxylic acid, 3,5-pyrazoledicarboxylic acid, 4,5-imidazoledicarboxylic acid, 2-pyrazinecarboxylic acid) have been screened for possible improvement of the catalytic efficiency, however, no improvement was observed. The inactivity of the complexes **1** and **2** in cyclohexane oxidation is most probably due to the presence of iron(III)–chloride bonds that are too strong to allow exchange with solvent molecules or reactants.

Fontecave et al. [46] have reported that the activation of the C-H bond by hydroperoxides requires the presence of exchangeable coordination sites, in order to allow the binding of the oxidant to the metal centre. Therefore, it was decided to evaluate the corresponding in situ $CF_3SO_3^-$ salts of compounds **1** and **2** (obtained by addition of $AgCF_3SO_3$ to the methanol solution of **1** or **2**, followed by stirring and filtration through Celite to remove the silver salt) for the oxidation of cyclohexane. Using the procedure II, the maximum catalytic activity is reached after 3 h and it results in the formation of 3.2 equiv. cyclohexanol and 1.4 equiv. cyclohexanone in the reaction catalyzed by **1** and 1.8 equiv. cyclohexanol and 1.2 equiv. cyclohexanone in the reaction catalyzed by **2**. The use of the procedure I does not lead to any catalytic activity. Also, H_2O_2 dismutation has not been observed in both complexes.

By using a large excess of H_2O_2 (100 to 1000 equiv. in procedure II) neither cyclohexane conversion nor H_2O_2 dismutation activity was observed. In order to gain insight into the total lack of activity of complexes **1** and **2** under these conditions, the oxidation attempts were also followed by UV–Vis and ES-MS spectroscopy. The UV–Vis spectra of both compounds in methanol solution show similar features and no significant changes are observed when the solutions are kept at room temperature for several days. In both cases, the UV–Vis spectrum is dominated by a broad band at about 360 nm which is assigned to the iron-to-oxygen charge transfer transition. When H_2O_2 is added, the alkoxo-to-iron(III) LMCT band at 360 nm of **1** (356 nm for **2**) starts to decrease in intensity and to shift to higher energy; however in the presence of 10–20 equiv. H_2O_2, only insignificant changes are observed. When the amount of H_2O_2 added is increased, the intensity of the band decreases progressively and the band disappears completely after addition of 1000 equiv. of H_2O_2. The observed spectroscopic changes observed for compound **1** are presented in Fig. 5. This behaviour suggests a change in, or loss of, the coordination of the pyrazole ligand. Indeed, after addition of 1000 equiv. of H_2O_2, the ES-MS mass spectrum of complex **1** shows a peak at $m/z = 113$ with an abundance of 100% corresponding to the free Hnhep ligand and some other peaks of low intensity (abundance <10%) that could not be clearly assigned. A similar ES-MS mass spectrum was observed for complex **2** after addition of H_2O_2 (m/z = 141 $[Hnhed + H]^+$, 176 $[(H_2nhed)Cl + H]^+$).

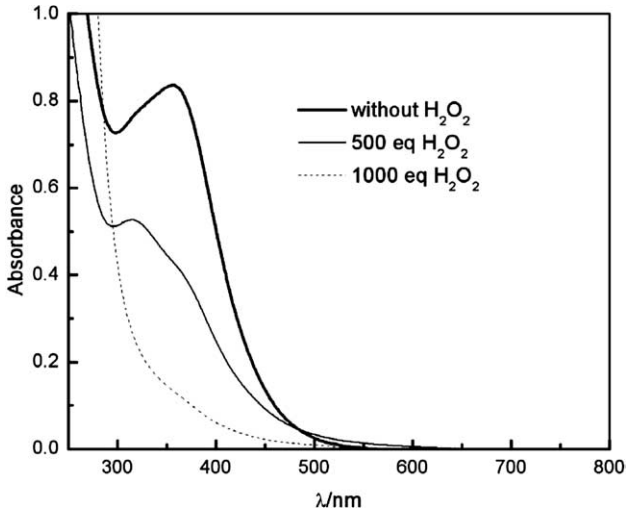

Fig. 5. Spectroscopic changes observed for a methanol solution of compound **1** upon the addition of H_2O_2.

4. Conclusions

We have synthesized and characterized two new bis(μ-alkoxo)diiron(III) complexes, $[Fe(nhep)Cl_2(EtOH)]_2$ (**1**) and $[Fe(nhed)Cl_2]_2$ (**2**) which have been inspired by the methane monooxygenase enzyme. The structural analysis of both complexes demonstrates the ability of the 1-(2-hydroxyethyl)pyrazole ligands to form dinuclear iron(III) compounds with a coordination number of five or six at the metal centre. A detailed characterization of complexes **1** and **2** including structural, spectroscopic and magnetic studies has been carried out. Replacing chloride ions with non-coordinating anions ($CF_3SO_3^-$) in compounds **1** and **2**, results in apparent catalytic activity in the oxidation of cyclohexane. This observation suggests that the inactivity of these complexes appears to be partly due to the presence of iron(III)-chloride bonds that are too strong to allow exchange with solvent molecules or reactants. Further optimization of the reaction conditions and the investigation of other substrates are in progress.

5. Supplementary material

Crystallographic data (excluding structure factors) have been deposited with the Cambridge Crystallographic Data Centre as supplementary publication no. CCDC 216734 (for **1**) and CCDC 223689 (for **2**). Copies of the data can be obtained free of charge on application to The Director, CCDC, 12 Union Road, Cambridge, CB2 1EZ, UK (fax: +44-1223-336-033; e-mail: deposit@ccdc.cam.ac.uk or www.ccdc.cam.ac.uk).

Acknowledgements

This work was in part financially supported by the Dutch Economy, Ecology, Technology (EET) programme, a joint programme of the Ministry of Economic Affairs, the Ministry of Education, Culture and Science, and the Ministry of Housing, Spatial Planning and the Environment. We thank Dr. R. Hage (Unilever, The Netherlands) for useful discussions.

References

[1] J.B. Vincent, G.L. Olivier-Lilley, B.A. Averill, Chem. Rev. 90 (1990) 1447.
[2] L. Que, A.E. True, Prog. Inorg. Chem., Bioinorg. Chem. 38 (1990) 97.
[3] B. Meunier, W. Adam, Metal-oxo and Metal-peroxo Species in Catalytic Oxidations, Springer, Berlin, 2000.
[4] J. Reedijk, E. Bouwman, Bioinorganic Catalysis, Marcel Dekker, New York, 1999.
[5] M.H. Baik, M. Newcomb, R.A. Friesner, S.J. Lippard, Chem. Rev. 103 (2003) 2385.
[6] D. Riley, M. Stern, J. Ebner, The Activation of Dioxygen and Homogeneous Catalytic Oxidation, Plenum, New York, 1993.
[7] R.A. Leising, J.H. Kim, M.A. Perez, L. Que, J. Am. Chem. Soc. 115 (1993) 9524.
[8] M. Costas, K. Chen, L. Que, Coord. Chem. Rev. 200 (2000) 517.
[9] R.A. Sheldon, J.K. Kochi, Metal-Catalyzed Oxidations of Organic Compounds, Academic Press, New York, 1981.
[10] J.B. Vincent, J.C. Huffman, G. Christou, Q.Y. Li, M.A. Nanny, D.N. Hendrickson, R.H. Fong, R.H. Fish, J. Am. Chem. Soc. 110 (1988) 6898.
[11] L. Que, Y.H. Dong, Accounts Chem. Res. 29 (1996) 190.
[12] H. Toftlund, Coord. Chem. Rev. 94 (1989) 67.
[13] R. Mukherjee, Coord. Chem. Rev. 203 (2000) 151.
[14] R.H. Fish, M.S. Konings, K.J. Oberhausen, R.H. Fong, W.M. Yu, G. Christou, J.B. Vincent, D.K. Coggin, R.M. Buchanan, Inorg. Chem. 30 (1991) 3002.
[15] R.A. Leising, R.E. Norman, L. Que, Inorg. Chem. 29 (1990) 2553.
[16] R.A. Leising, B.A. Brennan, L. Que, E. Munck, J. Am. Chem. Soc. 113 (1991) 3988.
[17] R.A. Leising, Y. Zang, L. Que, J. Am. Chem. Soc. 113 (1991) 8555.
[18] I.L. Finar, K. Utting, J. Chem. Soc. (1960) 5272.
[19] W.L. Driessen, E. Bouwman, Inorg. Synth. 32 (1998) 82.
[20] O. Kahn, Molecular Magnetism, VCH Publishers, New York, 1993.
[21] A.L. Spek, PLATON, A Multi-purpose Crystallographic Tool, Utrecht University, The Netherlands, 2003.
[22] P.T. Beurskens, G. Beurskens, R. de Gelder, S. García-Granda, R.O. Gould, R.I. Israel, J.M.M. Smits, The DIRDIF99 Program System, Technical Report of the Crystallography Laboratory, University of Nijmegen, The Netherlands, 1999.
[23] G.M. Sheldrick, SHELXL-97. Program for Crystal Structure Refinement, University of Göttingen, Germany, 1997.
[24] G.M. Sheldrick, SHELXL-97. Program for Crystal Structure Solution, University of Göttingen, Germany, 1997.
[25] G.B. Shul'pin, The Chemistry Preprint Server (www.chemceb.com/orgchem/0106001).
[26] E.I. Solomon, T.C. Brunold, M.I. Davis, J.N. Kemsley, S.K. Lee, N. Lehnert, F. Neese, A.J. Skulan, Y.S. Yang, J. Zhou, Chem. Rev. 100 (2000) 235.

[27] J.A. Bertrand, P.G. Eller, Inorg. Chem. 13 (1974) 927.
[28] A.B.P. Lever, Inorganic Electronic Spectroscopy, Elsevier Science, Amsterdam, 1986.
[29] S. Tanase, E. Bouwman, W.L. Driessen, J. Reedijk, R. de Gelder, Inorg. Chim. Acta 355 (2003) 458.
[30] H. Aneetha, K. Panneerselvam, T.F. Liao, T.H. Lu, C.S. Chung, J. Chem. Soc., Dalton Trans. 16 (1999) 2689.
[31] J.M. Clemente-Juan, C. Mackiewicz, M. Verelst, F. Dahan, A. Bousseksou, Y. Sanakis, J.P. Tuchagues, Inorg. Chem. 41 (2002) 1478.
[32] N.S. Goncalves, L.M. Rossi, L.K. Noda, P.S. Santos, A.J. Bortoluzzi, A. Neves, I. Vencato, Inorg. Chim. Acta 329 (2002) 141.
[33] A. Neves, L.M. Rossi, I. Vencato, W. Haase, R. Werner, J. Chem. Soc., Dalton Trans. 5 (2000) 707.
[34] H. Duval, V. Bulach, J. Fischer, M.W. Renner, J. Fajer, R. Weiss, J. Biol. Inorg. Chem. 2 (1997) 662.
[35] R.C. Finn, J. Zubieta, J. Clust. Sci. 11 (2000) 461.
[36] A. Horn, A. Neves, A.J. Bortoluzzi, V. Drago, W.A. Ortiz, Inorg. Chem. Commun. 4 (2001) 173.
[37] M. Pawlicki, L. Latos-Gralynski, Inorg. Chem. 41 (2002) 5866.
[38] J. Simaan, S. Poussereau, G. Blondin, J.J. Girerd, D. Defaye, C. Philouze, J. Guilhem, L. Tchertanov, Inorg. Chim. Acta 299 (2000) 221.
[39] L.J. Bellamy, A.J. Owen, Spectrochim. Acta A 25 (1969) 329.
[40] A.W. Addison, T.N. Rao, J. Reedijk, J. van Rijn, G.C. Verschoor, J. Chem. Soc., Dalton Trans. 7 (1984) 1349.
[41] E. Rentschler, G.A. Timco, T. Weyhermuller, V.B. Arion, A.S. Batsanov, J. Inorg. Biochem. 86 (2001) 398.
[42] S.M. Gorun, S.J. Lippard, Inorg. Chem. 30 (1991) 1625.
[43] J.A. Bertrand, J.L. Breece, A.R. Kalyanaraman, G.J. Long, W.A. Baker, J. Am. Chem. Soc. 92 (1970) 5233.
[44] G.J. Long, J.T. Wrobleski, R.V. Thundathil, D.M. Sparlin, E.O. Schlemper, J. Am. Chem. Soc. 102 (1980) 6040.
[45] W.M. Reiff, G.J. Long, W.A. Baker, J. Am. Chem. Soc. 90 (1968) 6347.
[46] S. Menage, J.M. Vincent, C. Lambeaux, M. Fontecave, J. Mol. Catal. A Chem. 113 (1996) 61.